Threading Bis-Intercalation of a Macrocyclic Bisacridine at Abasic Sites in DNA: Nuclear Magnetic Resonance and Molecular Modeling Study†

Muriel Jourdan, Julian Garcia,* and Jean Lhomme

LEDSS, Chimie Bioorganique, UMR CNRS 5616, Université Joseph Fourier, BP 53, 38041 Grenoble Cedex 9, France

Marie-Paule Teulade-Fichou, Jean-Pierre Vigneron, and Jean-Marie Lehn

Laboratoire de Chimie des Interactions Moléculaires, UPR 285, Collège de France, 11 place Marcelin Berthelot 75005 Paris, France

Received May 14, 1999; Revised Manuscript Received August 17, 1999

ABSTRACT: The macrocyclic bisacridine (CBA) has been reported previously to specifically recognize single-stranded nucleic acid structures, especially DNA hairpins. The binding of the drug with an abasic site-containing oligonucleotide, was investigated by ^{1}H NMR and molecular modeling. We have used a DNA undecamer, the d($C_1G_2C_3A_4C_5X_6C_7A_8C_9G_{10}C_{11}$)·d($G_{12}C_{13}G_{14}T_{15}G_{16}T_{17}G_{18}T_{19}G_{20}C_{21}G_{22}$) duplex in which the X residue is a stable analogue of the abasic site [3-hydroxy-2-(hydroxymethyl) tetrahydrofuran]. Analysis of the NMR data reveals that the bisacridine molecule forms two different intercalation complexes in a 80/20 (± 10) ratio. For the major complex, a molecular modeling study was performed guided by nineteen intermolecular drug−DNA restraints, determined from NOESY spectra. In this model, the ligand interacts in the threading binding mode with an acridine ring intercalated between the C_7-A_8 and $T_{15}-G_{16}$ base pairs, while the other acridine ring resides in the abasic pocket. The two linker chains are positioned in the minor and in the major groove, respectively. A comparable study was performed to evaluate the interaction of CBA with the parent unmodified duplex in which X_6 was replaced by an adenine residue. No complex formation was observed when operating in identical conditions. This shows the selective binding of CBA to the abasic site and its potential interest to target the abasic site lesion.

Abasic site formation, i.e., release of a nucleic base leaving a 2′-deoxyribose residue is the most frequent DNA damage that may occur in the cell by a variety of processes. Depurination occurs spontaneously with the highest frequency (*1*), a reaction that is markedly accelerated under the action of alkylating drugs (*2*, *3*) and ionizing radiations (*3*, *4*). Abasic sites are also produced in vivo in the base excision repair (BER) pathway (*5*−*8*) by specific glycosylases as intermediates in the repair of damaged or modified bases. The abasic sites so generated are removed enzymatically by AP-endonucleases by cleavage of the DNA strand at both sides of the abasic site followed by insertion of the proper nucleotide unit in the gap so produced. Two major classes of AP-endonucleases are known. Class I AP-endonucleases, or AP-lyases (*9*−*11*), cleave the phosphodiester bond on the 3′ side of the abasic site by a β-elimination mechanism leaving an α,β-unsaturated carbonyl derivative at the 3′-terminus. The class II AP-endonucleases cleave hydrolytically the phosphodiester bond on the 5′ side of the abasic site (*12*). Being noninformative lesions, abasic sites are mutagenic or lethal (*13*−*15*). Abasic sites repair is thus a critical cellular activity. Indeed anticancer drugs possessing alkylating properties such as nitrosoureas have been reported to create abasic sites at high frequency in tumor cells, a property that is considered to be related to the mode of action (*16*, *17*). It is thus of high interest to design molecules capable of interacting specifically at abasic sites in DNA, either as probes for the detection of the damage, or as drugs to interfere with the repair process, and explore the abasic site as a possible target for antitumor agents. Different types of compounds have been reported along these lines. 9-Aminoellipticines (*18*, *19*), 3-aminocarbazole (*20*, *21*), the tripeptide Lys−Trp−Lys (*22*−*24*), different polyamines (*25*) have been studied as incising agents at abasic sites mimicking the AP-lyase activity. Hybrid molecules, including a reporter moiety linked to an oxyamino unit, have been engineered by us (*26*) and others (*27*) as probes to detect abasic sites, based on the specific reactivity of the oxyamino function with the aldehydic abasic site. Very few compounds, however, have been reported, that bind the abasic site and act as AP-endonuclease inhibitors. 9-aminoellipticine (*28*), an acridine dimer (*29*) and a bisnaphthalimide DMP 840 (*30*) gave encouraging results, the latter being in phase I clinical trials. We recently reported molecules (DTAc and ATAc, Chart 1) that recognize abasic sites with high selectivity and cleave abasic plasmid DNA at nanomolar concentrations

† This work was supported by the Association pour la Recherche sur le Cancer (ARC) and the Ligue Nationale contre le Cancer (LA LIGUE).

* To whom correspondence should be addressed. Telephone: 33 (0)4 76 51 45 23. Fax: 33 (0)4 76 51 43 82. E-mail: julian.garcia@ujf-grenoble.fr.

[1] Abbreviations: AP, apurinic and apyrimidinic; δppm, chemical shift in parts per million; NOE, nuclear Overhauser effect; NOESY, two-dimensional nuclear Overhauser effect spectroscopy; DQFCOSY, double-quantum-filtered correlation spectroscopy; TOCSY, total homonuclear correlated spectroscopy; rMD, restrained molecular dynamic.

10.1021/bi991111h CCC: $18.00 © 1999 American Chemical Society
Published on Web 10/07/1999

Chart 1

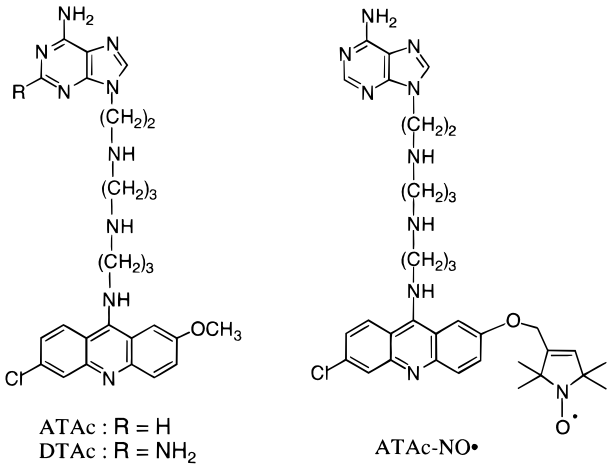

Chart 2 Chemical Structure and Numbering Scheme of Bisacridine (CBA).

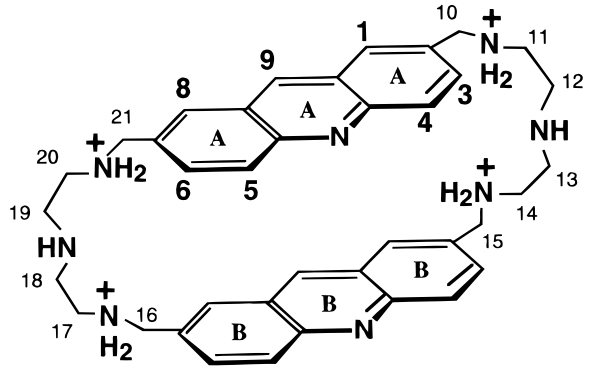

(*31*−*38*). These molecules were more recently shown to act as inhibitors of abasic site repair and potentiate the action of the anticancer drug BCNU (*39*) (*N*,*N*′-bis(2-chloroethyl)-*N*-nitrosourea). They bind to abasic DNA by inserting the nucleic base unit inside the abasic pocket, the acridine moiety intercalating at a two base pairs distance 5′ from the abasic site with the polyaminolinker lying in the minor groove (*38*). Quite interestingly, these molecules were also shown to bind uracyl bulges in RNA structures (*40*).

Bulges and abasic sites in duplexes share the common feature of presenting an extra base in one strand devoid of complementary base in the opposite strand. We recently reported that the cyclobisacridine (CBA) recognizes unpaired bases in DNA (*41*) being able to discriminate between single- and double-stranded structures (*42*−*44*). This suggested CBA as a novel candidate structure for targeting the abasic site lesion. CBA (Chart 2) is a member of a new class of artificial receptor molecules cyclo-bisintercalands, in which two DNA-intercalator subunits are linked by two polyammonium chains in such a geometry that small planar substrates can insert and stack between the two acridine units that constitute the walls of the macrocyclic cavity. On that basis, the cyclo-bisintercalator can accommodate a nucleic base in single-stranded DNA, while binding to a duplex structure is severely disfavored by the strain that would result from insertion of the two intercalating units between two successive base pairs (nearest neighbor exclusion principle) and by steric clashes of the two linkers with the sugar−phosphate backbone. Cleavage experiments conducted on a ^{32}P-labeled oligo-

Chart 3 DNA Duplex Containing the Tetrahydrofuran Analog X (top) and the Parent Unmodified Oligonucleotide (bottom).

$^{5'}$d(C$_1$ G$_2$ C$_3$ A$_4$ C$_5$ X$_6$ C$_7$ A$_8$ C$_9$ G$_{10}$ C$_{11}$)$^{3'}$
$^{3'}$d(G$_{22}$ C$_{21}$ G$_{20}$ T$_{19}$ G$_{18}$ T$_{17}$ G$_{16}$ T$_{15}$ G$_{14}$ C$_{13}$ G$_{12}$)$^{5'}$

$^{5'}$d(C$_1$ G$_2$ C$_3$ A$_4$ C$_5$ A$_6$ C$_7$ A$_8$ C$_9$ G$_{10}$ C$_{11}$)$^{3'}$
$^{3'}$d(G$_{22}$ C$_{21}$ G$_{20}$ T$_{19}$ G$_{18}$ T$_{17}$ G$_{16}$ T$_{15}$ G$_{14}$ C$_{13}$ G$_{12}$)$^{5'}$

X =

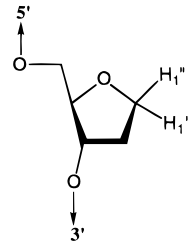

nucleotide (23-mer) containing an abasic site have shown that CBA incises DNA at the site of the lesion with moderate efficiency as compared to the AP-endonuclease mimics ATAc and DTAc (*45*). This suggests interaction at the abasic site. Unequivocal data, however, were obtained by examining the binding of CBA to the duplex oligonucleotide that contains a stable analogue of the abasic site X (Chart 3) in the middle of the sequence. This analogue X is known to retain the biological properties of the "true" abasic site (*46*). A melting temperature increase $\Delta T_m = +14$ °C was measured at a 1/1 ratio of drug per oligonucleotide and no further variation of the melting temperature was observed in the presence of excess drug. No modification of the melting temperature could be detected for the parent unmodified duplex (Chart 3) in the same conditions (*45*). In addition, CBA displaces the labeled heterodimer ATAc−NO• (Chart 1) from the abasic duplex as evidenced by EPR spectroscopy (*45*). Alternatively irradiation of a ^{32}P-labeled oligonucleotide (23-mer) containing the model abasic site X in the presence of CBA leads to selective photocleavage in the abasic site region (*45*). In the present paper, we report on the structure of the complex formed between CBA and the duplex oligonucleotide containing the stable analogue of the abasic site X in the middle of the sequence. The abasic site is flanked by two cytosine residues and is located opposite thymine. High field NMR spectroscopy and restrained molecular dynamics show that CBA behaves as a threading bisintercalator that forms a major specific 1/1 complex at the site of the lesion. The molecule penetrates between the base pairs of the duplex, sandwiching in the intercalation mode the G−C base pair on 3′ to the abasic site, with the two polyamino linkers lying respectively in the minor and in the major groove.

MATERIALS AND METHODS

Sample Preparation. The abasic site-containing undecamer was synthesized and purified as described previously (*47*) and the parent unmodified duplex was purchased from Eurogentec and purified like the abasic DNA duplex. The oligonucleotide duplexes were chromatographed over chelex 100 resin to remove dicationic metal ions. The NMR samples

were lyophilized once from water, twice from 99.96% D_2O, and finally dissolved in 600 μL of 99.99% D_2O, containing 20 mM sodium phosphate buffer at pH 5.8. For NMR experiments involving exchangeable protons, the oligomers were dissolved in 90 H_2O/10% D_2O. The final duplex concentrations were about 1.5 mM.

The bisacridine (2, 5, 8, 21, 24, 27-hexaaza(9, 9)(2, 7)-acridinophane) was synthesized as reported previously (*41*). A dilute stock solution was prepared by dissolving 1.3 mg of this drug in 65 μL of 99.96% D_2O. Known amounts of bisacridine were added to the sample containing duplex DNA in 0.25 molar equiv per increment and the complete complex formation was monitored by 1D NMR.

NMR Experiments. NMR data sets were recorded on a Varian Unity Plus 500 and Varian Unity 600 spectrometers at temperature of 1 or 10 °C. Chemical shifts were referenced to the chemical shift of water, which had been calibrated relative to the 3-(trimethylsilyl)propionate-2, 2, 3, 3-d_4 (TSP-d_4). All 2D NMR experiments in D_2O were performed using the standard pulse sequences with presaturation of the residual HOD signal during the relaxation delay and during the mixing time for the NOESY. The NOESY spectra with mixing times of 90 and 250 ms were obtained using 2048 complex points in t_2, and 300 t_1 increments with 64 or 128 scans for each t_1 value. The TOCSY experiment with a mixing time of 60 ms was acquired with 2048 complex points in t_2 and 300 increments in t_1 with 64 transient for each FID. The DQFCOSY spectrum was run with 2048 points in t_2, 400 points in t_1, and 128 scans for each t_1 values. The NOESY in 90% H_2O was carried out by replacing the first pulse of the standard sequence with a 270° composite pulse (*48*) and the observation pulse with a 1−1 jump and return pulse to suppress the solvent signal (*49*). A total of 4092 complex points were collected in t_2, 300 points in t_1, and 128 scans for each FID.

All the data were processed with a Gaussian window function prior to Fourier transformation and zero-filled in t_1.

Distance Restraints and Molecular Modeling. Intermolecular NOE cross-peaks were integrated and converted to distance restraints in the two-spin approximation. There has not been performed any attempt to correct the NOEs for the presence of spin diffusion. A total of 19 intermolecular drug−DNA NOEs were measured and classified semiquantitatively into three categories: strong (2.0−3.0 Å), medium (3.0−4.0 Å), and weak (4.0−5.0 Å). Energy minimizations and restrained molecular dynamics (rMD) were performed using the Discover version 97.0 software (Biosym/Molecular Simulation) (*50*) with the AMBER force-field potential (*51*). In the dynamic calculations, the ends of the duplex (i.e., C_1-G_{22} to A_4-T_{19} and C_9-G_{14} to $C_{11}-G_{12}$) were fixed in B-DNA conformation. Distance restraints with a force constant of 100 kcal mol^{-1} Å^{-2} were included to enforce Watson−Crick hydrogen bond for C_5-G_{18} and A_8-T_{15}. No force constant was introduced to ensure C_7-G_{16} base pairing. An upper and lower bound force constant of 25 kcal mol^{-1} Å^{-2} was assigned for experimentally derived NOE restraints and a distance-dependent dielectric function of $\epsilon = 4r$ was used to account for solvent effects. First, the canonical B-form (*52*) of the intercalation site-containing oligonucleotide was built using the Builder module of Insight II. Then, the drug was manually docked into the DNA duplex. The complex was initially energy-minimized using 100 and 2000 cycles of steepest descent and conjugate gradients, respectively. Then, 32 ps of restrained molecular dynamics with the following temperature profile was applied: 600 K for 4 ps cooled to 250 K in 50 K steps of 4 ps each. The system was maintained at 250 K for an additional 4 ps. The final structure was then energy minimized using conjugate gradient under restrained conditions. Finally, the structure was released from all constraints and subsequently energy-minimized to a maximum derivative of 0.01 Å. No distance violation greater than 0.2 Å was observed.

The final structure was analyzed using the CURVES version 5.1 (*53*, *54*) software.

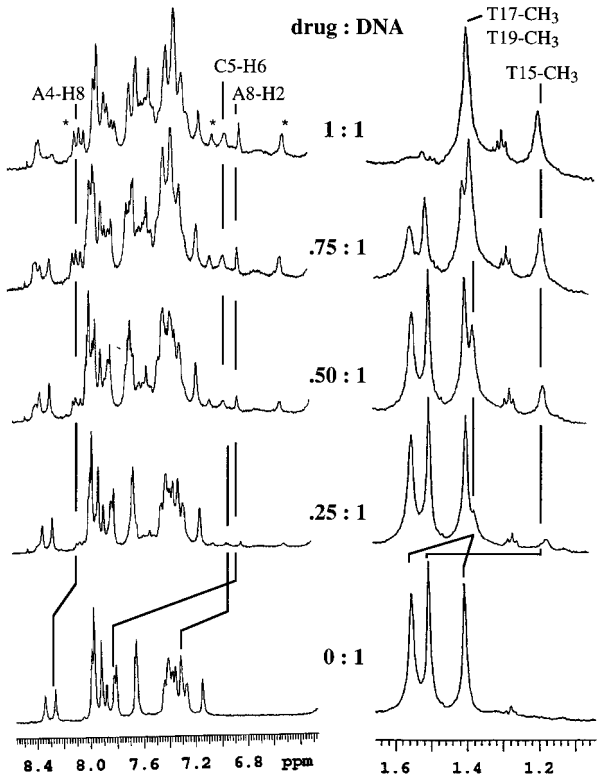

FIGURE 1: 1D NMR spectra corresponding to the aromatic and thymine methyl regions of the abasic site-containing DNA upon the addition of CBA in D_2O, at 10 °C and at pH 5.8. The molar drug−DNA ratios are indicated for each spectrum. The solid lines follow some representative DNA resonances during the titration. The peaks denoted with dots are from the drug molecule.

RESULTS

CBA−DNA Complex Formation. One-dimensional ^{1}H NMR spectra of the aromatic and methyl regions of the complex, at different drug−DNA ratios, are shown in Figure 1. Progressive addition of CBA led to doubling of resonances over much of the spectrum. With an increasing amount of drug, resonances from the original undecamer spectrum decreased, disappearing completely when a 1/1 ratio was reached, while new resonances increased. This effect was particularly clear for the thymine methyl groups and for many of the aromatic base protons. The different spectra shown in Figure 1 were obtained at 10 °C and indicated a slow exchange regime. The three original methyl resonances were replaced by two new signals showing unequal intensities. The first at 1.40 ppm integrated for more than two methyl groups and the second one at 1.20 ppm for less than one

methyl group. This and other features in the spectrum proved that two different complexes were present in solution. Furthermore, several exchange cross-peaks were observed in the 250 ms NOESY and TOCSY spectrum. This implies slow exchange on the chemical shift time scale between the two different 1/1 drug−DNA complexes. It is worth noting that the base pairs undergoing chemical exchange were those adjacent to the abasic site and those located on the 3′-side (i.e., A_4-T_{19} to $G_{10}-C_{13}$). Integration of many exchange cross-peaks in the TOCSY spectrum indicated a proportion of 80/20 (± 10%) between the two complexes at 10 °C. This corresponds to a difference in stability of about $\Delta\Delta G° = -3$ kJ mol^{-1}. The exchange rate between these two complexes was estimated from the line width of the methyl group at 1.20 ppm relative to the line width of original DNA. It was assumed that the broadening of this peak was essentially due to kinetic effect and short lifetime of the drug at a particular site. Thus, this measure gave an upper limit of the exchange rate. Using the relation $\Delta\upsilon = (\pi\tau)^{-1}$, where $\Delta\upsilon$ is the line width increase and τ the lifetime of the drug, we found at 10 °C a value of 30 ms as lower limit for the lifetime of the drug in a specific binding site. Because of extensive broadening of the resonances, we could not rule out the presence of other complexes that could represent less than 10% of the total.

Proton Assignments of Free CBA. The resonances of CBA appeared to be very dependent on pH. Thus, proton assignments were carried out at pH 5.8 similar to that used for the drug−DNA complex study. Because of the symmetry of the molecule, the ^{1}H NMR spectrum of the free CBA is solely constituted of four CH aromatic and three methylene protons. However, when bound to DNA, it is expected that all these protons could be in different environments with different chemical shifts. Resonances of the free drug were unambiguously assigned by a combination of 1.2 s NOESY and spin decoupling experiments. The attributions are given in Table 1.

Nonexchangeable Proton Assignments for the Major CBA−DNA Complex. NMR assignments for the free undecamer have been reported in an earlier work (*47*).

The proton resonances of the oligonucleotide in the complex were assigned in a sequential manner using NOESY, DQFCOSY, and TOCSY spectra following the well-established strategy described for right-handed DNA duplexes (*55*−*57*). The attributions are listed in Table 2.

Figure 2 shows the aromatic and sugar region for the nonexchangeable protons of a 250 ms NOESY spectrum from which the sequential assignment was deduced. It was possible to follow the distance connectivities monitoring the NOEs between the base (H8 or H6) protons and their own and 5′-flanking sugar protons. Furthermore, sequential base−base connectivities were also observed in the aromatic region and confirmed the proposed attributions. However, two interruptions of the sequential connection were noticed in the oligonucleotide. Obviously, due to the lack of a base at the X_6 site, the X_6 base to C_5-H1' NOE was missing. Nevertheless, NOEs, weaker than similar patterns were detected for the $T_{17}-H1'/G_{18}-H8$ counterpart, located on the opposite strand. This result testified that the distance between the C_5 and X_6 residues remained relatively short. On the other hand, no internucleotide NOE was detected between C_7-H1'/A_8-H8 and $T_{15}-H1'/G_{16}-H8$, which is a clear evidence of intercalation of one acridine unit between the C_7-G_{16}/A_8-T_{15} base pairs. Identification of C_7 and G_{16} was not easily performed at this stage since no internucleotide NOE was observed for these two nucleotides. Thus, C_7 was assigned on the basis of its strong H5−H6 cross-peaks present in the NOESY and DQFCOSY spectra, while G_{16} was identified as the remaining base not yet attributed and presenting intranucleotide correlations only. The A_4-H2 and A_8-H2 protons were readily distinguished from the other base protons in a one-dimensional inversion−recovery experiment (data not shown). The abasic sugar resonances were assigned from DQFCOSY and NOESY spectra. The H1′/H1″ protons were identified at 4.19 and 4.09 ppm, respectively on the basis of their cross-peak intensities with the abasic H3′ proton in the 90 ms NOESY spectrum.

Table 1: ^{1}H Chemical Shift and NOESY Cross-Peaks of CBA in the Major 1/1 CBA−DNA Complex[a]

proton	free	bound	$\Delta\delta$[b]	CBA−DNA NOEs[c]
Acr-H1A	7.84	7.41	−0.43	
Acr-H3A	7.57	7.69	0.12	
Acr-H4A	7.86	7.60	−0.26	C_5-H2' (s)
Acr-H5A	7.86	7.30	−0.56	
Acr-H6A	7.57	7.40	−0.17	
Acr-H8A	7.84	7.15	−0.69	
Acr-H9A	8.71	8.12	−0.88	$G_{18}-H1$ (m) $G_{16}-H1$ (m)
CH_2-10	4.04	4.33	+ 0.29	
CH_2-11	3.29	3.39	+ 0.10	
CH_2-12	3.11	3.28	+0.17	
CH_2-13	3.11	3.18/3.09		
CH_2-14	3.29	3.53	+ 0.24	
CH_2-15	4.04	4.29/4.10	+0.25/+0.06	$T_{15}-CH_3$ (m)
CH_2-16	4.04	4.54/4.49	+0.50/+0.45	A_8-H4' (m) A_8-H1' (s)
CH_2-17	3.29	3.28		
CH_2-18	3.11	3.11/3.02		
CH_2-19	3.11	3.18		C_7-H1' (s)
CH_2-20	3.29	3.38		
CH_2-21	4.04	4.33/4.28	+0.29/+0.24	
Acr-H1B	7.84	6.20	−1.64	$T_{15}-H2''$ (s)
Acr-H3B	7.57	7.50		$T_{15}-CH_3$ (s)
Acr-H4B	7.86	7.43	−0.43	$T_{15}-CH_3$ (m)
Acr-H5B	7.86	6.52	−1.34	C_7-H2'(w) C_7-H2'' (w) C_7-H1'(w) C_7-H_5 (w) C_7-H_6 (w)
Acr-H6B	7.57	6.24	−1.53	C_7-H2' (w) C_7-H2'' (m) C_7-H1' (w)
Acr-H8B	7.84	7.69	−0.15	
Acr-H9B	8.71	7.88	−0.83	A_8-H2 (m)

[a] H_2O is referenced at 4.97 ppm. Proton assignments are at 10 °C. [b] $\Delta\delta = [\delta(\text{complex}) - \delta(\text{CBA})] \geq 0.10$ ppm. [c] s = strong, m = medium, and w = weak intensity.

Interaction of CBA with the duplex resulted in dramatic line broadening and variation of chemical shifts, relative to free DNA. However, the greatest changes occurred at the central part of the sequence, i.e., around the abasic site (C_5-G_{18} to A_8-T_{15}). For example, one of the most striking effects was the upfield shift of the C_5-H6 and H5 protons that have moved by 0.36 and 0.85 ppm respectively, when compared to free DNA. A similar behavior was observed for the A_8-H2 proton that was shielded by 1 ppm, with respect to the free DNA. From the variations of the nonexchangeable proton chemical shifts, it remained impossible to position the second acridine ring.

The CBA protons in the complex were assigned following analysis of the NOESY, TOCSY, and DQFCOSY data sets in D_2O solution. As expected, binding of the drug to the DNA duplex caused both the acridine and the methylene

Table 2. ^{1}H Chemical Shift Assignments of the DNA Resonances in the Major 1/1 CBA-DNA Complex[a]

residue	H8	H6	H5/Me/H2	H1′	H2′	H2″	H3′	H4′	imino[b]	amino[c]
C1		7.63	5.90	5.74	1.99	2.42	4.72	4.08		na
G2	7.96			5.87	2.66	2.78	4.72 (−0.29)	4.27 (−0.11)	13.04	
C3		7.35	5.41	5.58	2.04	2.35	4.84	4.36 (−0.14)		8.32/6.48 (−0.12/−0.11)
A4	8.07 (−0.21)		7.54 (−0.28)	6.06 (−0.18)	2.47 (−0.22)	2.73 (−0.16)	4.83 (−0.20)	4.19 (−0.73)		
C5		6.96 (−0.36)	4.40 (−0.85)	5.51 (−0.41)	2.23	2.45 (0.25)	4.68 (−0.18)	4.18		7.37/6.00 (−0.73/−0.57)
X6				4.09/4.19[d] (0.10/0.29)	2.21 (0.22)	2.30 (0.31)	4.82 (0.24)			
C7		7.54 (−0.12)	5.58 (−0.33)	5.82 (0.26)	2.28 (0.30)	2.49	4.83			7.38[e]/6.11[e] (−0.97/−0.8)
A8	8.40		6.86 (−0.98)	6.00 (−0.18)	2.70	2.84	4.89 (−0.93)	4.36		
C9		7.24	5.15(−0.18)	5.48 (−0.11)	1.97	2.30	4.82	4.19		7.99/6.48 (−0.26/−0.19)
G10	7.82			5.94	2.58	2.73	4.81 (−0.19)	4.26	12.99 (−0.15)	
C11		7.36	5.28	6.13	2.20	2.20	4.51	4.00		na
G12	7.93			5.95	2.63	2.78	4.84	4.27	na	
C13		7.35 (−0.15)	5.28 (−0.11)	5.73	2.10	2.41	4.83	4.51 (0.28)		8.33/6.48 (−0.17/−0.14)
G14	7.80 (−0.18)			5.88 (−0.13)	2.56 (−0.10)	2.66 (−0.12)	4.88 (−0.12)	4.35	12.48 (−0.44)	
T15		7.05 (−0.11)	1.20 (−0.31)	6.06 (0.27)	2.11 (0.21)	2.40 (0.14)	4.35 (−0.54)	4.26	12.58 (−1.34)	
G16	7.96 (0.12)			5.96	2.69	2.69	4.85	4.19	10.27[e] (−2.55)	
T17		7.29 (−0.10)	1.40 (−0.18)	5.92	2.31 (0.25)	2.52 (0.23)	4.93		na	
G18	8.03			6.00	2.72	2.79	4.45 (−0.49)	4.36	11.88 (−0.85)	
T19		7.29	1.40	5.72 (−0.15)	2.22	2.52	4.82	4.34 (0.12)	13.57 (−0.25)	
G20	7.88			5.82	2.62	2.71	4.83 (−0.17)	4.36	12.67 (−0.15)	
C21		7.35	5.43	5.72	1.92	2.36	4.84	4.51 (0.31)		8.47/6.66
G22	7.93			6.14	2.63	2.37	4.70	4.18	na	

[a] H_2O is referenced at 4.97 ppm. Proton assignments are at 10 °C, pH 5.8 (at 600 MHz). Values in parentheses represent chemical shift changes from free undecamer ≥0.10 ppm ($\Delta\delta = \delta$(complex) − δ(DNA)). [b] Assignments of H1 imino protons of guanine and of H3 imino protons of thymine. [c] Assignments of hydrogen-bonded amino protons and exposed amino protons of cytosine. [d] Assignments of H1′ and H1″ protons of the abasic site. [e] Assigned at 1 °C. na = Not assigned.

protons to become nonequivalent, thus having different chemical shifts. The aromatic region of the DQFCOSY spectrum displayed four sets of vicinal coupling connectivities corresponding to the Acr-H3, H4, and Acr-H5 and H6 protons of the two acridine moieties. The Acr-H1 and Acr-H8 protons were identified on the basis of their long-range coupling constants with the Acr-H3 and H6 protons, respectively. The two Acr-H9 protons were assigned from their NOE cross-peaks to both Acr-H1 and H8 protons. The methylene protons of the linker chains were identified by combined use of TOCSY and NOESY cross-peaks. The CH-10 and CH-21 methylene protons gave intense NOEs to the Acr-H1A, H3A and Acr-H6A, H8A protons, respectively, thus providing a convenient starting point for assignment of the chain resonances. Similar correlations were observed for the second acridine ring.

Upon complexation, most of the acridine peaks were broadened and moved upfield up to 1.6 ppm. These changes are typical of intercalation in the duplex.

To monitor the effect of CBA on the stability of the oligonucleotide, we followed the chemical shift variations of the thymine methyl protons as a function of temperature. We found a melting profile transition of 60 °C corresponding to a value approximately 15 °C higher than that obtained for this duplex in the absence of drug (47) (data not show).

Exchangeable Proton Assignments for the Major CBA−DNA Complex. Figure 3 shows the one-dimensional NMR spectrum corresponding to the imino proton region of the free and complexed DNA. Severe line broadening arising from the equilibrium between competing complexes was observed. As a general feature, we noticed that all resonances have moved upfield relative to free DNA.

The imino and amino protons were assigned following analysis of the NOESY spectrum of the complex recorded in H_2O at 10 °C. The chemical shift values are given in Table 2. The observed cross-peaks permitted correlation between the guanine imino with the hydrogen-bonded and exposed cytosine amino protons, which in turn showed NOEs with the nonexchangeable H5 cytosine proton. The thymine iminos exhibited strong NOEs with the adenine H2 protons and weak NOEs with their corresponding methyl protons. These cross-peaks are characteristic of normal Watson−Crick base pairing. Additional imino−imino NOEs between flanking base pairs were also noticed throughout the duplex. However, these sequential connectivities were disrupted at the abasic site and between C_7-G_{16} and A_8-T_{15}. In fact, at a temperature of 10 °C the G_{16} imino signal was dramatically exchange broadened and could not be assigned. This signal became sharper when decreasing the temperature to 1 °C enabling its assignment in the NOESY spectrum as for the other imino protons.

It is noteworthy that the imino protons of three base pairs display large upfield shifts. Indeed, the G_{18}, T_{15}, and G_{16} imino resonances are shifted upfield by 0.8, 1.3, and 2.5 ppm, respectively. These findings account for bis-intercalation of CBA. One of the two acridine moieties is inserted in the abasic pocket between C_5-G_{18} and C_7-G_{16} and the other is intercalated between C_7-G_{16} and A_8-T_{15}, the C_7-G_{16} base pair being sandwiched between the two drug chromophores. The G_{16} imino proton displays medium NOEs with reso-

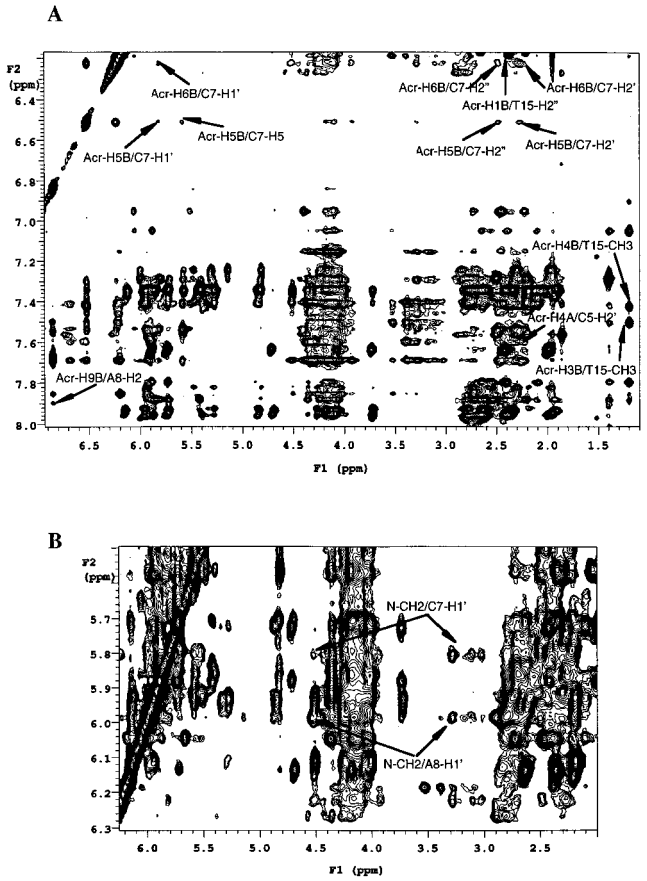

FIGURE 2: Expanded NOESY map (250 ms, 600 MHz) showing the aromatic to sugar protons region (A) and the deoxyribose H1′ to H2′ region (B). Selected intermolecular drug−DNA cross-peaks are indicated.

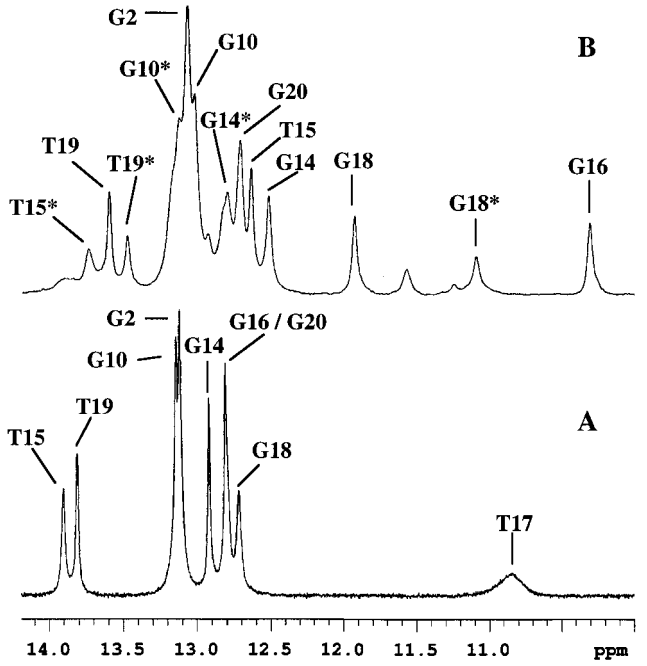

FIGURE 3: 1D NMR spectra (500 MHz, 10 °C) of the imino protons corresponding to the free DNA (A) and to the CBA-DNA complex (B). Resonances due to the minor complex are marked with asterisks. Note the upfield shifts of the T_{15}, G_{16} and G_{18}, imino protons.

nances at 7.38, 6.11, and 5.58 ppm, which were assigned to the aminos and H5 proton of the C_7 residue, respectively. This result indicate that the C_7-G_{16} base pair is stabilized at least partially by Watson−Crick pairing. The T_{17} imino proton was not detected nor were the exchangeable protons of the drug.

Intermolecular Contacts Between CBA and DNA. Complete assignment of the drug and oligonucleotide resonances provided the basis for identifiying drug−DNA contacts, and thus for deducing the mode of binding of CBA. The NOESY spectrum shown in Figure 2 displayed several intermolecular drug−DNA cross-peaks that allowed identification of the binding site. In the major complex the NOE contacts were found between the drug and the central C_5-G_{18} to A_8-T_{15} base pairs. This indicated that the interaction site of CBA is in the abasic site region. Several NOE cross-peaks were observed between Acr-H3B and Acr-H4B protons and the T_{15} methyl group. The Acr-H5B and Acr-H6B protons presented, in turn, NOE contacts with the C_7 nucleotide. These NOEs were consistent with intercalation of one acridine dye between the C_7-G_{16} and A_8-T_{15} base pairs. Fewer NOE contacts were detected for the other acridine residue. These involved the Acr-H4A proton with the C_5 nucleotide on one hand and the Acr-H9A and Acr-H1A protons with the $G_{18}-H1$ imino proton, on the other hand. These interactions indicate that the second acridine moiety is located inside the abasic site pocket. The CH_2-16 protons of one linker chain exhibited NOEs with the anomeric and H4′ protons of A_8. Similar NOEs were observed between the CH_2-19 protons on the same chain and the anomeric C_7 proton (Figure 2). These data indicate that this chain is located in the minor groove. The other chain, i.e. CH_2-15, displayed interaction with the T_{15} methyl group, which requires the second chain to be placed in the major groove.

Table 1 presents the intermolecular NOESY cross-peaks and their relative intensities observed for the major drug−DNA complex.

Structural Characterization of the Minor CBA−DNA Complex. The 250 ms NOESY spectrum of the 1/1 CBA−DNA solution displayed a second set of connectivities possessing lower intensities corresponding to a minor complex. Several exchange cross-peaks were observed between the two complexes. The nucleotides involved in this exchange were those corresponding to the A_4-T_{19} to $G_{10}-C_{13}$ part and no exchange cross-peaks were detected between the C_1-G_{22} to C_3-G_{20} base pairs. However, it was not possible to follow the sequential connectivities due to low abundance and to important line broadening. For the same reasons, no intermolecular drug−DNA NOEs were observed.

It is noteworthy that in the minor complex the A_8-H2 resonance exhibits a chemical shift value equivalent to that of A_4-H2. In other words, the shielding effect observed in the major complex for A_8-H2 and arising from intercalation of the acridine ring is no longer observed in the minor form. Furthermore, close inspection of the 250 ms NOESY spectrum run in H_2O revealed also a second set of connectivities for the imino/amino resonances corresponding to the minor form (Table S1, Supporting Information). In this spectrum, we observed exchange cross-peaks between the two complexes for the A_4-T_{19} to C_5-G_{18} base pairs and for the A_8-T_{15} to $G_{10}-C_{13}$ residues. In the minor complex, the imino proton of C_5-G_{18} is shielded by 1.6 ppm, while those of the A_8-T_{15} to $G_{10}-C_{13}$ part have moved upfield only slightly with respect to free DNA. Since no exchange

cross-peak involving the exchangeable protons of G_2-C_{21} to A_4-T_{19} residues was detected, we concluded that in the minor complex an acridine moiety is intercalated in the abasic pocket, whereas the position of the second acridine could not be defined.

Interaction Between CBA and the Parent Unmodified Duplex. To study the binding selectivity of CBA toward the abasic site we added the drug to parent undecamer possessing identical sequence in which the abasic site is replaced by adenosine. We used the same experimental conditions as those used for the abasic site-containing oligonucleotide. The ^{1}H NMR spectrum showed neither significant line broadening nor variations in the chemical shifts of the DNA and CBA resonances. It can be confidently concluded that no binding occurs between the drug and "regular" DNA.

DISCUSSION

Because of the presence of competing complexes and because of the few intermolecular NOEs available, it is not possible to make a quantitative study. However, we performed a molecular modeling study guided by NMR restraints to obtain a model of CBA binding mode that would agree with the NMR data. The most important results can be summarized as follows.

Sequence Specificity and Multiple Conformations. Analysis of the NMR spectra reveals that CBA forms two different intercalation complexes with the abasic site-containing undecamer. These complexes are present in a 80/20 (±10%) ratio and are in slow to intermediate exchange on the chemical shift time scale. The exchange rate between the two complexes has been estimated from line width analysis to be less than 33 s^{-1} (i.e. lifetime higher than 30 ms). CBA binds exclusively in the C_5-G_{18} to A_8-T_{15} region of the DNA duplex. This is supported by the fact that the greatest DNA proton chemical shift differences were detected in the abasic site region. This specificity was further confirmed by the fact that no interaction between the drug and the fully paired undecamer was observed.

Intercalation Sites of CBA. The NMR results for the major complex show clear evidence that one of the two acridine residues (ring B) intercalates between the $C_7-G_{16}-A_8-T_{15}$ base pairs, while the other acridine moiety (ring A) inserts between the C_7-G_{16} and C_5-G_{18} base pairs. As a result, the G_{18}, T_{15}, and G_{16} imino protons are shielded by 0.8, 1.3, and 2.5 ppm, respectively, as compared to free DNA. The dramatic upfield shift experienced by the G_{16} imino proton is rationalized on the basis of combined ring-current effect of the two flanking acridine moieties. Detection of NOEs between T_{17} and G_{18} reveals that the second acridine moiety (ring A) does not stack between these two bases. On the other hand, no NOE is observed between $T_{17}-H6$ and $G_{16}-H1',H2'$, due to severe overlapping. On the complementary strand, similar overlapping does not allow observation of NOE between C_7 and X_6. Nevertheless, these observations do not indicate that CBA is stacked between T_{17} and G_{16}, since an intermolecular contact is detected between the drug and the G_{18} imino proton. Furthermore, the upfield shift of 0.8 ppm noticed for this proton is most likely the result of a close drug−DNA interaction, which would not be consistent with an intercalation occurring between G_{16} and T_{17}. In fact, at the abasic site level the acridine ring and T_{17} are almost in a same plane. Further evidence of CBA intercalation is given by the differences in chemical shifts of the aromatic protons in the free and bound molecules. On complexation, all acridine resonances, except Acr-H3A, are shifted upfield up to 1.6 ppm, which is characteristic of an intercalative binding mode (Table 1).

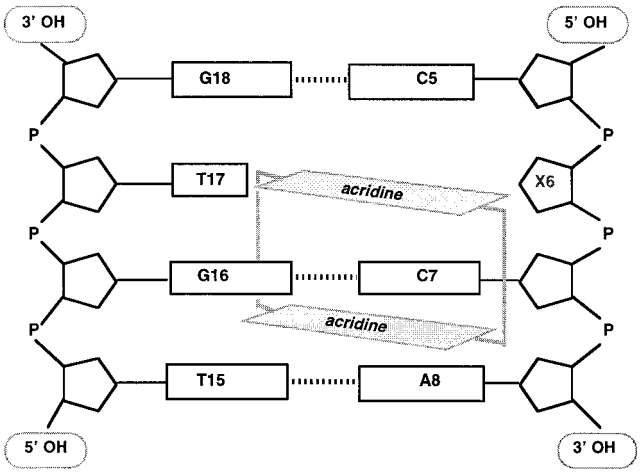

FIGURE 4: Schematic representation of the major CBA−DNA complex. The chromophores thread through the helix with the linker chains lying in either groove.

Linker Chains Binding. The NMR data indicate that the two linker chains bind in opposite grooves. Intermolecular NOEs are detected between one of the chains and the $A_8-H1',H4'$, and C_7-H1' resonances, which are minor groove markers. On the other hand, NOE contacts between the other linker and the T_{15} methyl group are observed, which allowed positioning of the second chain in the major groove. These findings suppose a threading binding mode for CBA, which is further supported by the intermolecular NOEs noticed for the two intercalating chromophores.

Structure of the Major CBA-DNA Complex. Nineteen intermolecular distance restraints have been determined from the NOESY spectra. These were used for performing a molecular modeling study to obtain a model of CBA binding mode that would agree with the NMR data. However, the presence of competing complexes and the small number of molecular NOEs available prevented complete quantitative analysis. A schematic representation of the complex is shown in Figure 4 and the structure obtained after dynamics calculations is given in Figures 5 and 6. The various views in Figure 6 show that the two acridine rings have quite different positions relative to their flanking base pairs. The long axis of the acridine moiety intercalated between C_7-G_{16} and A_8-T_{15} is oriented parallel to the long axis of the A_8-T_{15} residues. This chromophore stacks partially over its adjacent C_7 nucleotide, while no stacking is observed with the G_{16} residue. By contrast, the major axis of the second acridine moiety located in the abasic site pocket forms approximately a 90° angle with the major axis of the C_5-G_{18} base pair. In fact, this chromophore stacks with the bases located on one strand (i.e., C_5 and C_7) and not with their complementary counterpart (i.e., G_{16} and G_{18}). Similar partial overlap involving stacking of the drug with the two flanking bases on the same strand only has been described previously for threading intercalators such as nogalamycin (*58*). The two acridine moieties are oriented with the ring nitrogens pointing toward the major groove and the linking chains

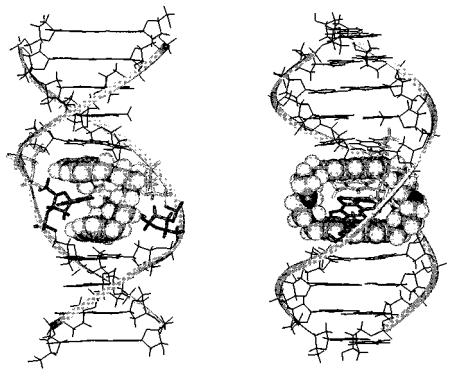

FIGURE 5: Molecular modeling based structure of the major CBA−DNA complex. The drug is drawn in CPK. Left: view from the major groove. Right: the same representation after a 90° angle rotation.

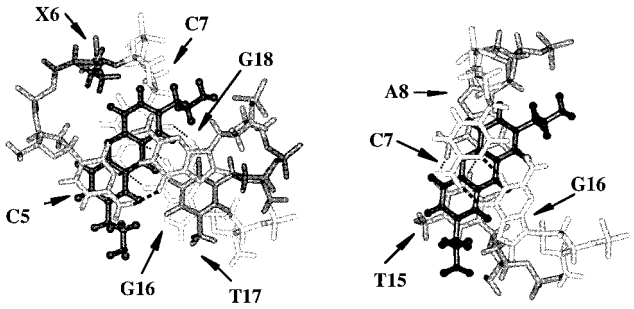

FIGURE 6: View looking down to the helical axis of the complexation site. These drawings emphasize the overlap geometries between the acridine moieties and their flanking base pairs. For clarity, only one acridine moiety is displayed in each picture. (A) Position of the acridine ring in the abasic pocket. (B) Position of the acridine ring at the $C_{7p}A_8$ ($T_{15p}G_{16}$) step.

positioned in the middle of each groove.

In the DNA duplex, the abasic sugar is pushed out away from the minor groove, while the T_{17} residue is slightly shifted toward the major groove, stacking partially with G_{16} (Figure 6A). The glycoside torsion angle of T_{17} remains roughly anti. The C_7-G_{16} base pair that is sandwiched between the two acridine rings exhibits substantial buckling up to 36° (Figure S1, Supporting Information). This conformation is likely to allow better stacking of the C_7 base with the acridine ring situated in the abasic site pocket (Figure 5).

Detailed inspection of the refined structure reveals the possible existence in the minor groove of one hydrogen bond between $C_{20}-NH_2^+$ and C_7-O2 (2.20 Å). In the major groove, two hydrogen bonds can be present between $C_{14}-NH_2^+$ and $G_{16}-N7$ (2.13 Å) and between $C_{10}-NH_2^+$ and $T_{17}-O4$ (2.34 Å). In addition to these intermolecular hydrogen bonds, other electrostatic interactions between the positively charged side chains and the negatively charged functional groups of the nucleotides in both grooves can contribute to the stabilization of the complex. These interactions may involve C_7-O2 (3.56 Å) and $G_{16}-N2$ (3.26 Å) in the minor groove and $G_{16}-O6$ (3.46 Å) in the major groove.

Determination of the Minor CBA Complex. The detection of intercalation site in the minor complex is more speculative. Analysis of the imino chemical shift indicates that no intercalation occurs between the C_7-G_{16} to $C_{11}-G_{12}$ residues. In contrast, the G_{18} imino proton is shifted upfield by 1.7 ppm and the T_{19} imino is shielded by 0.4 ppm. This result gives clear evidence that an acridine moiety is located in the abasic site. The chemical shift of the G_{18} imino proton for the minor form is quite different from that observed for the major form pointing out a different complexation geometry for the two complexes. A possible minor form is the one with one of the two chromophores intercalated in the abasic site and the other on 5′ side, i.e., between A_4-T_{19} and C_5-G_{18}. However, since the position of the second acridine moiety could not be defined precisely, it can also lie in the major or in the minor groove. Since neither the T_{17} nor the G_{16} imino protons could be detected for the minor form, intercalation of the second acridine ring between X_6-T_{17} and C_7-G_{16} cannot be ruled out, the T_{17} base being sandwiched between the two chromophores. Formation of the minor complex could result from intercalation of the first acridine ring in the abasic site, the second acridine ring remaining outside the duplex. Opening of the C_7-G_{16} base pair allows insertion of the second acridine ring between the C_7-G_{16} and A_8-T_{15} nucleotides giving the major complex. This seems a reasonable hypothesis, since the opening of a single base pair was previously demonstrated to be a rapid event, the imino proton half-lives being typically in the 1−40 ms range (*59, 60*).

CONCLUSION

Combined high-field NMR spectroscopy and restrained molecular dynamics calculations shed light on earlier observations showing specific binding of the cyclobisacridine CBA to abasic site structures in DNA (*45*). CBA incises DNA at the abasic site as demonstrated on a synthetic-labeled oligomer. All collected data obtained with duplex oligonucleotide containing the stable analogue X of the abasic site clearly indicated 1/1 complex formation. Strong stabilization of the abasic site-containing duplex was observed in the presence of CBA. This molecule displaced the abasic site specific EPR probe ATAC−NO• from the abasic site-containing duplex. The structure of the major CBA−DNA complex as detailed by the present NMR study explains these observations. The abasic lesion represents a site of strong thermodynamic destabilization for the duplex and of enhanced flexibility. CBA inserts at this site, penetrating the double helix, leading to stabilization as a result of π stacking interaction of the acridine rings with the base pairs and electrostatic interaction between the protonated amines of the linkers in the drug and the floor of the grooves. This gives rise to a unique structure of the threading intercalation mode for the complex. In addition, this geometry totally explains the photocleavage experiments that showed the G−C base pairs on both sides of the lesion to be selective cleavage sites in the ^{32}P-labeled oligonucleotide (23-mer) containing the stable analogue of the abasic site (*45*).

ACKNOWLEDGMENT

We thank Professor Jacques Reisse (Université Libre de Bruxelles, Belgium) for fruitful discussions and for giving us access to the 600 MHz Varian spectrometer. We also thank Miss Véronique Gineste for secretarial help.

SUPPORTING INFORMATION AVAILABLE

One table listing the proton chemical shift for the minor CBA-DNA complex and a schematic representation using

CURVES of the DNA duplex. This material is available free of charge via the Internet at http://pubs.acs.org.

REFERENCES

1. Lindahl, T., and Nyberg, B. (1972) *Biochemistry 11*, 3610−3618.
2. Singer, B., and Grunberger, D. (1983) *Molecular Biology of Mutagens and Carcinogens* ; Plenum Press: New York, pp 16−19.
3. Price, A. (1993) *Cancer Biology 4*, 61−71.
4. Teoule, R. (1987) *J. Radiat. Biol. 5*1, 573−589.
5. Laval, E., and Laval, F. (1980) *Molecular and Cellular Aspects of Carcinogens Screening Tests* ; Oxford University Press: Oxford, U.K., Vol. 27, pp 55−73.
6. Weiss, B., and Grossman, L. (1987) *Adv. Enzymol. Relat. Areas Mol. Biol*., *60*, 1−34.
7. Sancar, A., and Sancar, G. B. (1988) *Annu. Rev. Biochem. 57*, 29−67.
8. Myles, G. M., and Sancar, A. (1989) *Chem. Res. Toxicol. 2*, 197−226.
9. Bailly, V., and Verly, W. G. (1987) *Biochem. J. 242*, 565−572.
10. Kim, J., and Lin, S. (1988) *Nucl. Acids Res. 146*, 229−241.
11. Bailly, V., and Verly, W. G. (1989) *Nucl. Acids Res. 17*, 3617−3618.
12. Demple, B., and Harrison, L. (1994) *Annu. Rev. Biochem. 63*, 915−948.
13. Gentil, A., Margot, A., and Sarasin, A. (1984) *Mutat. Res. 129*, 141−147.
14. Loeb, L. A., and Preston, B. D. (1986) *Annu. Rev. Genet. 20*, 201−230.
15. Hickson, I. D. (1997) *Base Excision Repair of DNA Damage*, Springer-Verlag, Heidelberg, Germany, pp 81−102.
16. Lown, J. W., and McLaughlin, L. W. (1979) *Biochem. Pharmacol. 28*, 1631−1638.
17. Lown, J. W., Joshua, A. V., and McLaughlin, L. W. (1980) *J. Med. Chem. 23*, 798−805.
18. Malvy, C., Prevost, P., Gansser, C., and Paoletti, C. (1986) *Chem. Biol. Interact. 57*, 41−53.
19. Bertrand, J.-R., Vasseur, J.-J., Gouyette, A., Rayner, B., Imbach, J.-L., Paoletti, C., and Malvy, C. (1989) *J. Biol. Chem. 264*, 14172−14178
20. Vasseur, J.-J., Rayner, B., Imbach, J.-L., Verna, S., McCloskey, J. A., Lee, M., Chang, D. K., and Lown, J. L. (1987) *J. Org. Chem. 52*, 4994−4998.
21. Vasseur, J.-J., Peoc′h, D., Rayner, B., and Imbach, J.-L. (1991) *Nucleosides Nucleotides 10*, 107−117.
22. Behmoaras, T., Toulme, J.-J., and Hélène, C. (1981) *Nature 78*, 926−930.
23. Pierre, J., and Laval, J. (1981) *J. Biol. Chem. 256*, 10217−10220.
24. Hélène, C., Toulme, J.-J., Behmoaras, T., and Cazenave, C. (1982) *Biochimie 64*, 697−705.
25. Male, R., Fosse, V., and Kleppe, K. (1982) *Nucl. Acids Res. 20*, 6305−6308.
26. Boturyn, D., Boudali, A., Constant, J. F., Defrancq, E., and Lhomme, J. (1997) *Tetrahedron 53*, 5485−5492.
27. Liuzzi, M., Weinfeld, M., and Paterson, M. C. (1987) *Biochemistry 26*, 3315−3321.
28. Lefrançois, M., Bertrand, J.-R., and Malvy, C. (1990) *Mutation Res. 236*, 9−17.
29. Malvy, C., Pierre, J., Lefrançois, M., Markovits, J., Garbay, C., and Roques, B. P. (1990) *Chem.-Biol. Interact. 73*, 249−260.
30. O′Reilly, S., Baker, S. D., Sartorius, S., Rowinsky, E. K., Finizio, M., Lubiniecki, G. M., Grochow, L. B., Gray, J. E., Pieniazek, H. J. Jr, and Donehower, R. C. (1998) *Ann. Oncol. 9*, 101−104.
31. Constant, J.-F., O′Connor, T. R., Lhomme, J., and Laval, J. (1988) *Nucl. Acids Res. 16*, 2691−2703.
32. Fkyerat, A., Demeunynck, M., Constant, J.-F., Michon, P., Lhomme, J. (1993) *J. Am. Chem. Soc. 115*, 9952−9959.
33. Fkyerat, A., Demeunynck, M., Constant, J.-F., and Lhomme, J. (1993) *Tetrahedron 49*, 11237−11252.
34. Constant, J.-F., Fkyerat, A., Demeunynck, M., Laval, J., O′Connor, T. R., and Lhomme, J. (1990) *Anticancer Drug Design 5*, 59−62.
35. Berthet, N., Boudali, A., Constant, J.-F., Decout, J. L., Demeunynck, M., Fkyerat, A., Garcia, J., Laayoun, A., Michon, P., and Lhomme, J. (1994) *J. Mol. Recognition 7*, 99−107.
36. Belmont, P., Boudali, A., Constant, J.-F., Demeunynck, M., Fkyerat, A., Lhomme, J., Michon, P., and Serratrice, G. (1997) *New J. Chem. 21*, 47−54.
37. Berthet, N., Constant, J.-F., Demeunynck, M., Michon, P, Lhomme, J. (1997) *J. Med. Chem. 40*, 3346−3352.
38. Coppel, Y., Constant, J.-F., Coulombeau, C., Demeunynck, M., Garcia, J., and Lhomme, J. (1997) *Biochemistry 36*, 4831−4843.
39. Barret, J. M., Fahy, J., Ethiévant, C., Lhomme, J., and Hill, B. T. (1999) *Anti-Cancer Drugs 10*, 55−65.
40. Wilson, W. D., Ratmeyer, L., Cegla, M. T., Spychala, J., Boykin, D., Demeunynck, M., Lhomme, J., Krishnan, G., Kennedy, D., Vinayak, R., and Zon, G. (1994) *New. J. Chem 18*, 419−423.
41. Teulade-Fichou, M. P., Vigneron, J. P., and Lehn, J. M. (1995) *Supramol. Chem. 5*, 139−147.
42. Slama-Schwok, A., Peronnet, F., Hantz-Brachet, E., Taillandier, E., Teulade-Fichou, M. P., Vigneron, J. P., Best-Belpomme, M., and Lehn, J. M. (1997) *Nucl. Acids Res. 25*, 2574−2581.
43. Slama-Schwok, A., Teulade-Fichou, M. P., Vigneron, J. P., Taillandier, E., and Lehn, J. M. (1995) *J. Am. Chem. Soc. 117*, 6822−6830.
44. Blacker, A. J., Teulade-Fichou, M. P., Vigneron, J. P., Fauquet, M., and Lehn, J. M. (1998) *Bioorg. Medic. Chem. Lett. 8*, 601−606.
45. Berthet, N., Michon, J., Teulade-Fichou, M. P., Vigneron, J. P., Lehn, J. M., and Lhomme, J. (1999) *Chem. Eur. J.*, in press.
46. Takeshita, M., Chang, C. N., Johnson, F., Will, S., and Grollman, A. P. (1987) *J. Biol. Chem. 262*, 10171−10179.
47. Coppel, Y., Berthet, N., Coulombeau, C., Coulombeau, Ce., Garcia, J., and Lhomme, J. (1997) *Biochemistry 36*, 4817−4830.
48. Freeman, R., Friedrich, and J., Xi-Li, W. (1988) *J. Magn. Reson. 79*, 561−567.
49. Plateau, P., and Gueron, M. (1982) *J. Am. Chem. Soc. 104*, 7310−7311.
50. Insight II 97.0/Discover 97.0 of Biosym/MSI 9685 Strandon Road-San Diego.
51. Weiner, S. J., Kollman, P. A., Nguyen, D. T., and Case, D. A. (1986) *J. Comput. Chem. 7*, 230−252.
52. Arnott, S., Chandrasekaran, R., Birdsall, D. L., Leslie, A. G. W., and Ratliff, R. L. (1980) *Nature (London) 283*, 743−745.
53. Lavery, R., and Sklenar, H. (1996) Curves 5.1 Manual, CNRS, Paris.
54. Lavery, R., and Sklenar, H. (1989) *J. Biomol. Struct. Dyn. 6*, 655−667.
55. Feigon, J., Leupin, W., Denny, W. A., and Kearns, D. R. (1983) *Biochemistry 22*, 5943−5951.
56. Scheek, R. M., Russo, N., Boelens, R., Kaptein, R., and Van Boom, J. H. (1983) *J. Am. Chem. Soc. 105*, 2914−2916.
57. Wüthrich, K. (1986) *NMR of Proteins and Nucleic Acids*, John Wiley and Sons, New York, pp 203−255.
58. Zhang, X.; Patel, D. J. (1990) *Biochemistry 29*, 9451−9466.
59. Kochoyan, M., Leroy, J.-L., and Gueron, M. (1987) *J. Mol. Biol. 196*, 599−609.
60. Leroy, J.-L., Kochoyan, M., Huynh-Dinh, T., and Gueron, M. (1988) *J. Mol. Biol. 200*, 223−238.

BI991111H